

# Internal and external morphology of adults of the appendicularian, *Oikopleura dioica*: an SEM study

Takeshi A. Onuma<sup>1</sup> · Miho Isobe<sup>1</sup> · Hiroki Nishida<sup>1</sup>

Received: 13 June 2016 / Accepted: 4 October 2016 / Published online: 11 November 2016  
© Springer-Verlag Berlin Heidelberg 2016

**Abstract** The appendicularian, *Oikopleura dioica*, is a planktonic tunicate that retains a swimming tadpole shape throughout its life. It has relatively few cells and exhibits fast development, yet it has a basic chordate body plan. In this study, the morphology of adults was investigated using scanning electron microscopy (SEM) and fine 3D images of most organs were taken. The trunk epidermis is organized into bilateral territories secreting the house that includes the food-trapping filter. The pharynx extends ventrally and posteriorly to the gill openings and esophagus, respectively. The endostyle, with a morphologically distinct ciliated band, is embedded in the pharynx. The digestive tract showed left–right asymmetry as the connection between the pharynx and esophagus tilts leftward. The heart is located ventrally between the left stomach and the intestine and consists of a left muscular sheet and a right thin, non-muscular sheet. The brain is connected to the oral and ventral sensory organs, ciliary funnels and sensory vesicles and axons descend from it that eventually innervate the caudal ganglion. In the tail, a nerve cord with sporadically distributed neuronal somata runs along the left side of the notochord. The gonad is a single syncytium of thousands of gametes. In the ovary, an abundance of cortical membrane invaginate into the cytoplasm during oogenesis and the growing oocytes are interconnected via common cytoplasm

through a ring canal. Spermatogenesis progresses synchronously within the common cytoplasm. These descriptions provide a valuable anatomical atlas for studying development and physiology using this simple organism with a chordate body plan.

**Keywords** SEM · Morphology · Appendicularian · Tunicate · Chordate

## Introduction

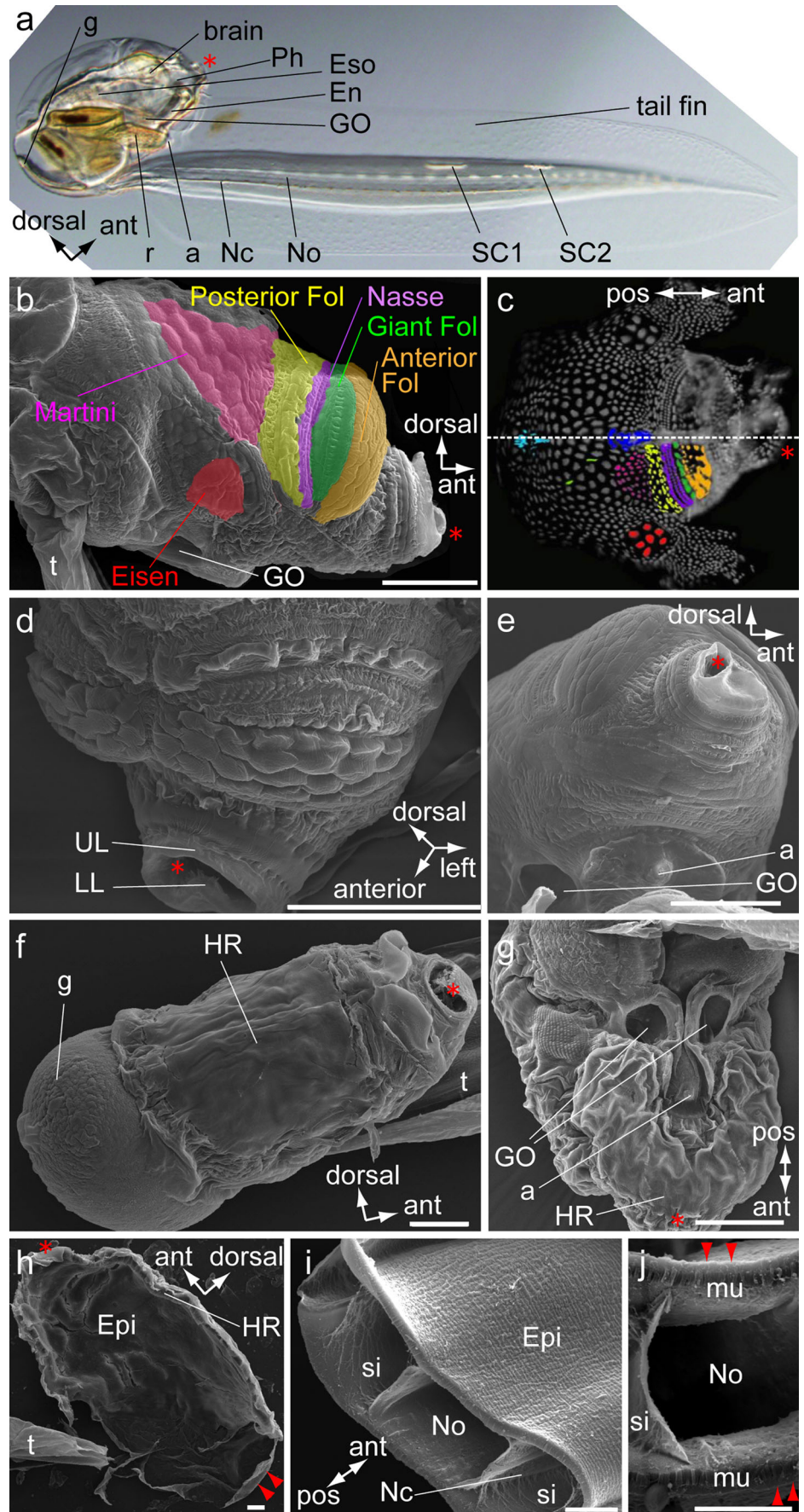
Appendicularians are marine planktonic tunicates that retain a swimming tadpole shape throughout their life (Fenaux 1998; Nishida 2008). Together with the ascidians and thaliaceans, they comprise a sister group to vertebrates (Delsuc et al. 2006; Nishida 2008). The appendicularian, *Oikopleura dioica*, represents a relatively simplified body plan for the chordates, which is characterized by a muscular tail with a notochord and neural tube and a trunk with an endostyle and gill openings on the ventral side (Fig. 1a). It has been proposed as a model organism for studies on chordate development for several reasons (Nishida 2008): (1) it has a short life cycle of 5 days at 20 °C; (2) its development is rapid and organ formation is complete within 10 h after fertilization, forming a functional body; (3) its morphogenesis and cell lineages before hatching are well described (Fujii et al. 2008; Nishida 2008; Stach et al. 2008; Nishida and Stach 2014; Stach and Anselmi 2015); (4) its body is transparent and live imaging is feasible (Clarke et al. 2007; Kishi et al. 2014); (5) its genome is compact at 70 Mb and its genome and transcriptome information are available (Seo et al. 2001; Denoed et al. 2010; Danks et al. 2013; Wang et al. 2015); and (6) knockdown methods via the introduction of morpholino oligonucleotide or double-stranded RNA and DNA have been established

**Electronic supplementary material** The online version of this article (doi:10.1007/s00441-016-2524-5) contains supplementary material, which is available to authorized users.

✉ Takeshi A. Onuma  
takeo@bio.sci.osaka-u.ac.jp

<sup>1</sup> Department of Biological Sciences, Graduate School of Science, Osaka University, 1-1 Machikaneyama-cho, Toyonaka, Osaka 560-0043, Japan

**Fig. 1** Epidermis and external morphology. **a** DIC image of live specimen. The trunk region is shown from the *right side*. The tail is skewed 90° to show the structures. *Asterisk* represents the mouth. **b–h** Oikoplasic epidermis of the trunk. **b** Right view. The oikoplasic regions were color-mapped. Each color corresponds to regions validated with DAPI staining of opened and flattened epidermis (**c**). The *dotted white line* in (**c**) represents the dorsal midline that passes through the mouth (*asterisk*) and the anterior and posterior rosette regions (*blue* and *light blue*, respectively). **d** Dorsal view. **e** Anterior ventral view. **f, g** Oikoplasic layers covered with house rudiments (*HR*). **f** Right view. **g** Ventral view. **h** Inside view. The oikoplasic epidermis is thicker than the epidermis that covers the gonad (*red arrowheads*). **i, j** Cutting planes of the tail. The tail epidermis (*red arrowheads*) is lined with a single flattened muscle cell. *Scale bars* (**b, d–g**) 100 μm, (**h–j**) 20 μm. *a* anus; *En* endostyle; *Epi* epidermis; *Eso* esophagus; *g* gonad; *GO* gill opening; *LL* lower lip; *mu* muscle; *Nc* nerve cord; *No* notochord; *Ph* pharynx; *r* rectum; *SC1* 1st subchordal cell; *si* sinus; *t* tail; *UL* upper lip



(Sagane et al. 2010; Omotezako et al. 2013, 2015). In the present study, we describe the morphological features of *Oikopleura dioica* to provide baseline knowledge about this species.

The anatomy of appendicularians has been reviewed in detail (Fenaux 1998; Nishida 2008) and many studies have described the cellular organization of the trunk epidermis (Ganot and Thompson 2002), digestive tract (Burighel and Brena 2001), endostyle (Olsson 1965; Fredriksson et al. 1985; Troedsson et al. 2007; Cañestro et al. 2008), nervous system (Cañestro et al. 2005; Søviknes et al. 2005, 2007), sensory organs (Bassham and Poslethwait 2005), ovary (Nishino and Morisawa 1998; Ganot et al. 2006, 2007) and testis (Flood 1978; Martinucci et al. 2005). These studies have been based on planar images collected by confocal microscopy or transmission electron microscopy (TEM). Scanning electron microscopy (SEM) is a powerful way to obtain high-resolution stereoscopic images (de Souza et al. 2008). In appendicularians, however, only a few studies have conducted SEM observations (Flood 1975; Fredriksson and Olsson 1991; Bassham and Poslethwait 2005; Nakashima et al. 2011). These studies have specifically focused on structures of the mouth and tail. SEM analysis of the whole body would not only provide a stereoscopic atlas but would also aid in gaining insight into the functional anatomy of this chordate.

In this study, external and internal morphologies of adult *O. dioica* were investigated using SEM. Several kinds of sample preparation techniques revealed fine structures of nearly all the organs, such as the trunk epidermis, pharynx, digestive tract, heart, brain, nerve cord, ovary and testis. These results basically support previous knowledge and also complement it with novel discoveries, such as a left–right asymmetry in the passage from pharynx to the esophagus and gill openings, connections of the brain with various organs and internal structure of the sensory vesicle. Furthermore, our observations have clarified that the coenocytic ovary possesses a number of plasma membrane invaginations during oogenesis.

## Materials and methods

### Sample collection and laboratory culture

Live wild animals were collected at Sakoshi Bay and Tossaki Port in Hyogo, Japan, by scooping surface seawater with a bucket. No specific permissions were required. *Oikopleura dioica* were sorted and cultured in the laboratory over generations as described previously (Bouquet et al. 2009; Omotezako et al. 2013). In brief, animals were reared in 10-L containers in a mixture of two kinds of artificial seawater (REI-SEA Marine, REI-SEA, Tokyo, Japan, and MARINE ART BR, Tomita Pharmaceutical, Tokushima, Japan) stirred with a paddle (15 rpm) at 20 °C and fed with the flagellates

*Isochrysis galbana* and *Rhinomonas reticulata*, the diatom *Chaetoceros calcitrans* and the cyanobacterium *Synechococcus* sp. In this condition, *O. dioica* become sexually mature and usually spawn on the fifth day post-fertilization.

*Oikopleura dioica* completes organogenesis and formation of a fully functional body by 10 h after fertilization at 20 °C (Nishida 2008) and the body organization of juveniles and adults is constant throughout its lifetime. The only exception is the gonad, which undergoes gametogenesis on day 5. In this study, we thus used adults at days 4–5.

### Sample preparation and SEM

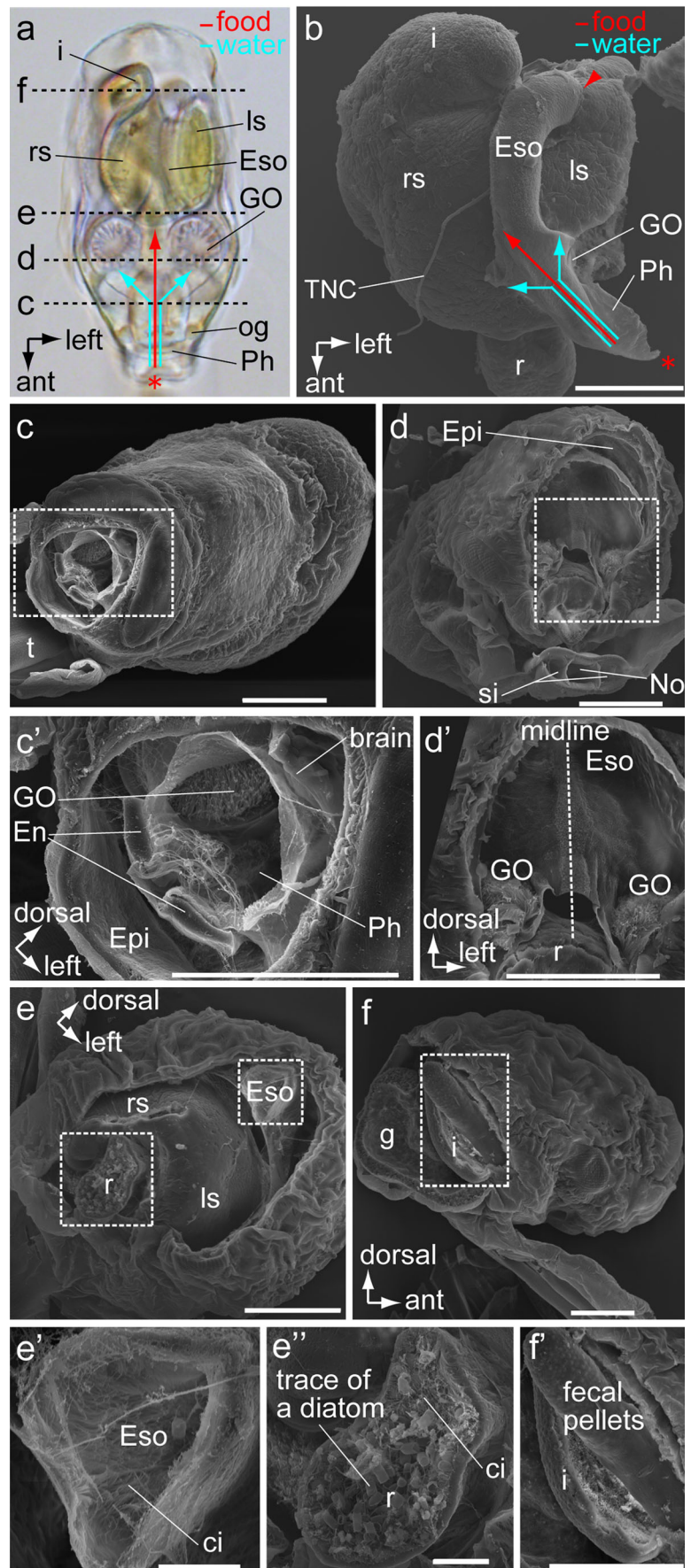
Animals were fixed overnight in 2.5% glutaraldehyde and 1% paraformaldehyde in the artificial seawater at 4 °C. Samples were then washed three times in distilled water, dehydrated in a graded ethanol series (50, 70, 90, 95 and 100 % for 5 min each) and subjected to critical point drying in a SAMDRI®-PVD-3D Critical Point Dryer (Tousimis, Rockville, MD, USA). The dried specimens were transferred to an adhesive tape on a specimen stub, coated with gold by an ION Sputtering Device JFC-1500 (JEOL, Tokyo, Japan) and then observed with a field emission SEM SU660 (Hitachi High-Technologies, Tokyo, Japan) operated at 15 kV accelerating voltage and 3.185 kV extraction voltage.

For SEM observations of the various organs, samples were prepared in different ways. To observe the trunk epidermis, inflated houses were removed by gentle pipetting of living animals. This treatment was repeated twice, immediately after the inflation of new houses, as the trunk epidermis is covered with a few layers of uninflated house rudiments. This enabled observation of the surface of the epithelial cells without house rudiments in less than 10 % of animals. The internal structures of the body were exposed in three different ways: (1) fixed samples were cut with a small razor blade; (2) the trunk epidermis of fixed animals was manually removed with tungsten needles; and (3) critical point dried specimens were fractured, which is a modification of the method described by Flood (1975). In brief, a piece of double-sided tape was pressed gently down on the dried animals that were taped on a specimen stub in various orientations. When the entire length of the trunk or tail adhered, the tape was carefully lifted away to peel off the epidermis and attached tissues to expose internal structures. The piece of tape was then turned upside down and placed beside the rest of the animal. To observe spermatids and spermatozoon, mature adults were transferred to a fixative solution, which induced the animals to immediately release all semen. The semen was left on glass slides coated with 0.1% poly-L-lysine for several hours for sperm cells to adhere to it.

Anatomical terms and abbreviations follow those used in previous publications (Fenaux 1998; Burighel and Brena 2001; Cañestro et al. 2005, 2008).



**Fig. 2** Digestive tract. **a, b** Dorsal views. **a** DIC image. *Asterisk* marks the mouth. *Red* and *blue arrows* depict flows of food and seawater, respectively. Seawater exits from a pair of gill openings (GO). See also Supplemental Movie S1. **b** An isolated digestive tract. *Red arrowhead* indicates connection point of the esophagus and left stomach. **c–f** Serial cutting planes from anterior to posterior levels viewed from the anterior (**c–e**) and posterior (**f**) sides. Corresponding level of each cutting plane is shown as *dotted lines* in (**a**). **c', d', e', e'', f'** Close-up views of the *square areas* indicated in (**c–f**). *Scale bars* (**b, c, c', d, d', e, f, f'**) 100  $\mu\text{m}$ , (**e', e''**) 20  $\mu\text{m}$ . \*mouth; *ci* cilium; *En* endostyle; *Epi* epidermis; *Eso* esophagus; *g* gonad; *GO* gill opening; *i* intestine; *ls* left stomach; *No* notochord; *Og* oral gland; *Ph* pharynx; *r* rectum; *rs* right stomach; *si* sinus; *t* tail; *TNC* trunk nerve cord



## Light and fluorescent microscopy and video recording

Nomarski (DIC) microscopy images of living animals were captured using an Olympus BX61 microscope. Animals were anesthetized using 0.015 % MS222 and mounted on a hollow glass slide. Movies were acquired using the DP2-BSW camera software (Olympus). DAPI staining of the trunk epidermis followed the methods of a previous study (Ganot and Thompson 2002) and serial sections of specimens that were embedded in resin (Technovit®) were stained with toluidine blue.

## Results and discussion

### Epidermis

The SEM images of the epidermis (Fig. 1) supported those of previous studies: the entire epidermis consists of a single layer of epithelial tissue and it has no mesodermal cells below (Nishida 2008). The trunk epithelial cells are highly patterned to secrete the house that includes the food-trapping filter and constitute the oikoplastic epithelium (Fenaux 1998). The epidermis is subdivided into bilateral symmetric territories (Fig. 1c), which are characterized by an invariant number of cells, cell sizes and cell shapes and specific gene expression (Ganot and Thompson 2002; Hosp et al. 2012). As shown in Fig. 1b, each territory has unique cell shapes. For instance, the anterior and giant Fol form a bump on the apical surface. Further, epithelial cell boundaries are obvious in the anterior portion of the trunk, except in the upper and lower lips (Fig. 1d, e).

The oikoplastic epithelium differs from other epidermal tissue in two ways. First, it is covered with the house rudiment (HR) (Fig. 1f, g). In the trunk, the dorsal epidermis is entirely covered with the HR (Fig. 1f). Likewise, the HR covers the anterior and ventral epidermis (Fig. 1g), reaching just behind the gill openings and anus. The HR does not exist on the posterior epidermis that covers the gonadal region (Fig. 1f, h, arrowheads) and tail epidermis (Fig. 1i, j). Second, the oikoplastic epithelium is much thicker than the other epidermises. The thickness of the oikoplastic epithelium is more than 10  $\mu\text{m}$  (Fig. 1h), whereas that of the gonadal epidermis and tail epidermis is less than 1  $\mu\text{m}$  (Fig. 1h, 1j). In a cross-section of the tail, the epidermis is recognized only as a very thin layer on the muscle (Fig. 1j, arrowheads). These results show that the oikoplastic epithelium and other epidermises have distinct structures reflecting different physiological roles as previously implicated by TEM observation (Burighel et al. 1989).

### Pharyngeal region and digestive tract

At the beginning of the digestive tract (Fig. 2), food and seawater enter the mouth and pass through the pharynx (Fig. 2a). Within the pharynx, food particles are trapped by mucus secreted from the endostyle and transported to the esophagus (Fig. 2a, b, red arrows). From here, the food progresses in sequence to the left stomach and right stomach before being delivered to the intestine, rectum and anus. Conversely, the seawater moves ventrally toward a pair of gill openings (Fig. 2a, b, blue arrows). In the gill openings, cilia beat to generate a water current into the body to draw food into the pharynx. This ciliary beating is readily visible in living animals (Supplemental Movie 1).

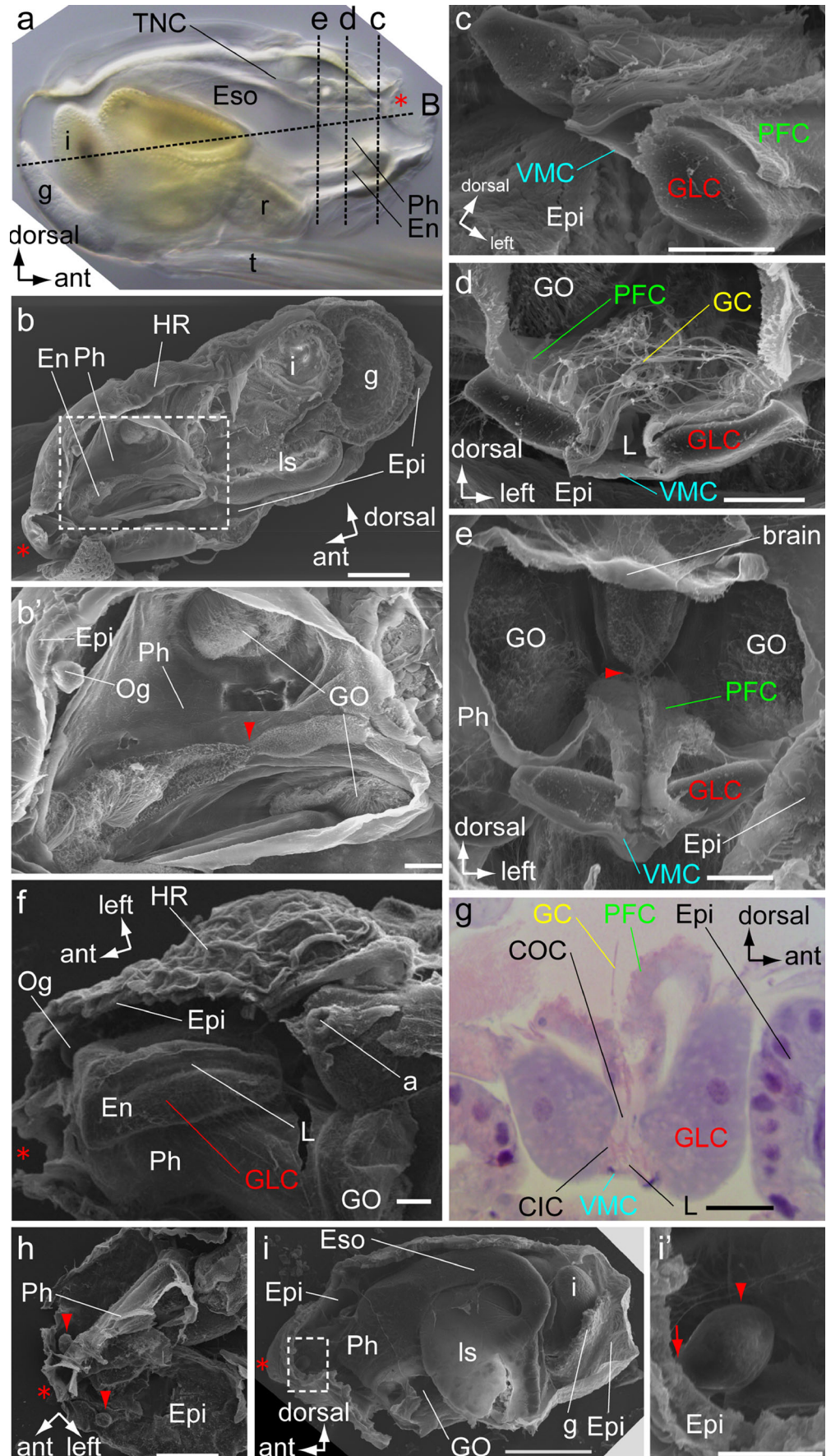
In the dorsal view, the pharynx forms a trigeminal passage consisting in the esophagus and a pair of gill openings (Fig. 2b). A ciliated ring locates ventrally to pass seawater toward the gill opening (Fig. 2c', d'). The esophagus is tube-shaped and situated along the anterior-posterior axis (Fig. 2b), lying between the oikoplastic epithelium and the dorsal surface of the stomach (Fig. 2e). It eventually curves to the left and is connected with the left stomach (Fig. 2b, arrowhead) and the passage to the esophagus tilts leftward to the midline (Fig. 2d') revealing the left-right asymmetry. In contrast, the two ciliated rings in the gill openings are located symmetrically on both sides (Fig. 2a, d').

Each region of the digestive tract has distinct internal morphology. In the esophagus, many cilia cover the internal wall (Fig. 2e'). In living animals, they beat continuously to draw food into the left stomach (Supplemental Movie 2) and cilia of distinct lengths also exist in the stomach (Fig. 4c), intestine (Fig. 2f') and rectum (Fig. 2e''). These cilia are considered to facilitate the propulsion of food particles (Burighel and Brena 2001). In the left stomach, roundish cells with short cilia are located in the inner wall (Fig. 4c) but they were not found in the right stomach. They are interpreted to be the globular cells, which have pinocytotic features and are proposed to absorb macromolecules (Burighel and Brena 2001). The intestine and rectum often contain fecal pellets (Fig. 2f'') and a trace of diatoms (Fig. 2e''), respectively. The rectum extends ventrally and thus the anus opened ventrally and anterior to a pair of the gill openings (Figs. 1b, g, 2d').

The endostyle (Fig. 3) is situated in the ventral part of the pharynx (Fig. 3a). It begins immediately behind the mouth and continues along the midline (Fig. 3a, b). In cross-sections, it is bilaterally symmetric and U-shaped (Fig. 3c–e). A remarkable feature is a pair of a single row of granular cells (GLC) that terminate posteriorly at the gill openings (Fig. 3b', e). On the apical surface, the pharynx floor plate cells (PFC) and numerous giant cilia (GC) are located on the GLC layer (Fig. 3c–e). The GC are dense in the anterior region but sparse or not found in the posterior region (Fig. 3b'). The PFC form a ciliated band that continues beyond the posterior



**Fig. 3** Endostyle and oral glands. **a** DIC image. Right view. **b–g** Endostyle. **b** Dorsal view of horizontal cutting plane. Close-up view of the square area is shown in **(b')**. **c–e** Serial cutting planes from anterior to posterior viewed from the anterior side. The corresponding level of each cutting plane is shown by the dotted lines in **(a)**. Arrowheads in **(b')** and **(e)** represent the posterior end of the glandular cell regions. **f** Ventral view of specimens from which the ventral epidermis is removed. **g** A cross resin section stained with toluidine blue. Glandular cell (*GLC*), pharynx floor plate cell (*PFC*), giant cilia (*GC*) and ventromedial cell (*VMC*) are labeled with red, green, yellow and light blue letters, respectively. **h, i** Oral glands (arrowheads). Dorsal view (**h**) and left view (**i**) of specimens from which the dorsal epidermis or left epidermis is removed, respectively. Detailed view of square area is shown in **(i')**. Oral gland connection with the epidermis (arrow). Scale bars (**b, h, i**) 100  $\mu$ m, (**b', c, d, e, f, g, i'**) 20  $\mu$ m. \*mouth; *a* anus; *CIC* ciliated cell; *COC* corridor cell; *En* endostyle; *Epi* epidermis; *Eso* esophagus; *g* gonad; *GC* giant cilia; *GLC* glandular cell; *GO* gill opening; *HR* house rudiments; *i* intestine; *L* lumen; *ls* left stomach; *Og* oral gland; *PFC* pharynx floor plate cell; *Ph* pharynx; *r* rectum; *t* tail; *TNC* trunk nerve cord; *VMC* ventromedial cell



end of the GLC, reaching the esophagus (Fig. 3b', e). On the basal side, thin ventromedial cells (VMC) form a ventral support structure and lumen (Fig. 3c–e). From the ventral view, the lumen is recognized as a groove (Fig. 3f). These structures are shown in different colors (see legend of Fig. 3) and coincide well with the serial resin section (Fig. 3g). In the vicinity of the mouth, the oral gland is present as a pair of large cells that are present between the endostyle and epidermis (Fig. 3h–i). The oral gland cells possess a round shape and smooth surface architecture (Fig. 3i') and the edge of the cells is attached to the epidermis (Fig. 3i').

## Heart

The heart is present ventrally between the left stomach and intestine (Fig. 4a–b) and is continuously beating (Supplemental Movies 1, 2, 3). The left and right walls are recognizable in the cross-section (Fig. 4a) and in the ventral view (Fig. 4b'). The left wall is composed of muscle fibers,

whereas the right wall is a non-muscular thin membrane and the surface architecture of the left wall is wavy, whereas that of the right wall is smooth (Fig. 4b', c). This coincides with the previous report that in two species, *O. rufescens* and *O. vanhoeffeni*, the left wall is composed of muscular cells (reviewed by Fenaux 1998). To our knowledge, the present study provides the first SEM images of the *Oikopleura* heart.

## Nervous system

The brain is present in the anterodorsal region adjacent to the pharynx (Fig. 5a) and consists in approximately 70 cells (Olsson et al. 1990; Søviknes et al. 2005, 2007; Cañestro et al. 2005). It links to the caudal ganglion (CG) of the tail through the trunk nerve cord (TNC) (Fig. 5a), which curves slightly right along the esophagus (Fig. 3a) and runs behind the bridge of the right and left stomachs (Fig. 2b) to enter the base of the tail (Fig. 5a). The brain is also connected to organs via various nerves (Figs. 5b', 6a). Paired nerves with sensory

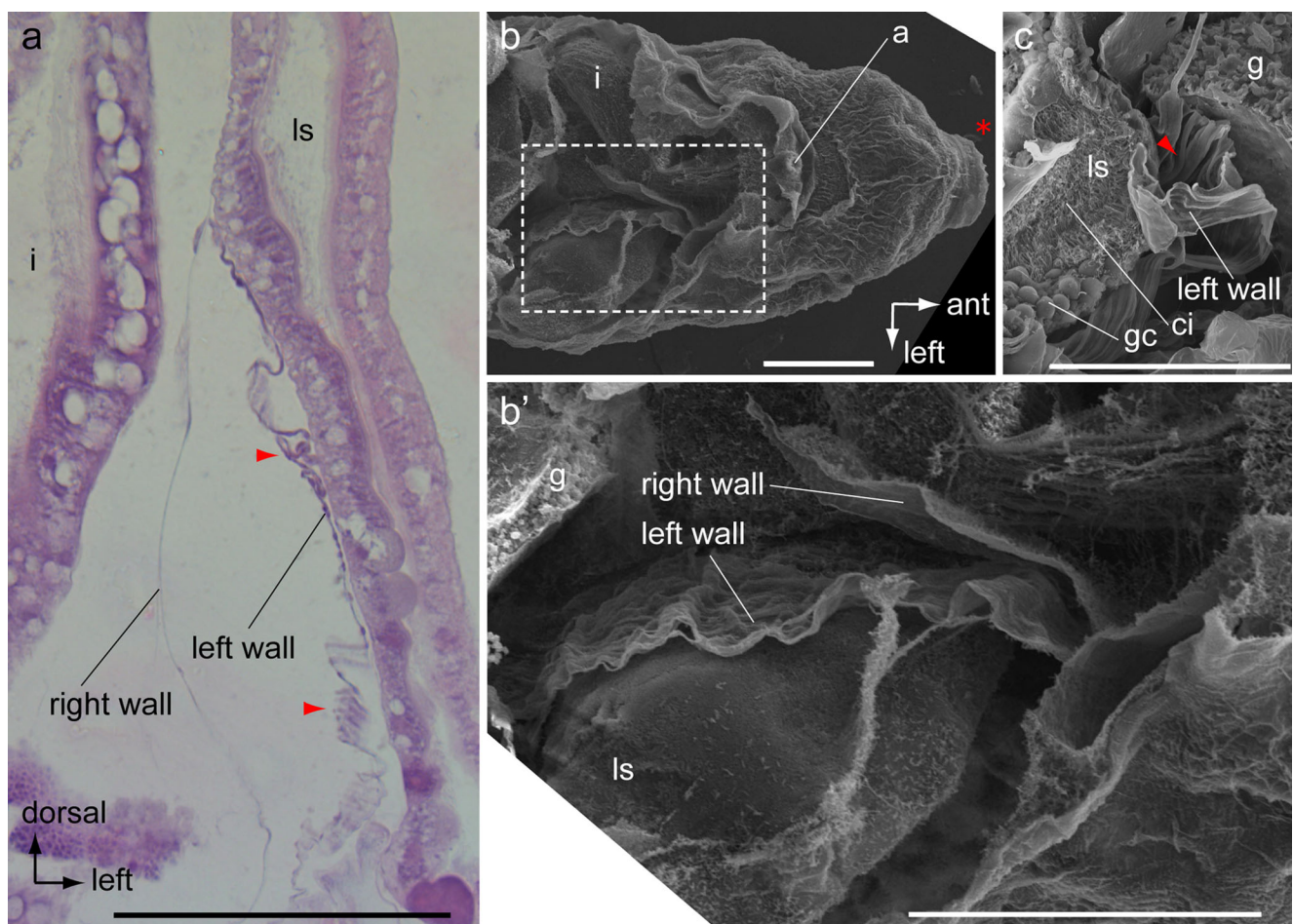


**Fig. 4** Heart. **a** Cross resin section stained with toluidine blue. Arrows indicate muscle fibers in the left wall. **b** Ventral view of specimens from which a portion of the ventral epidermis is removed. Asterisk the mouth. **b'** Detailed view of the square area in (b). **c** Dorsal view of horizontal

cutting plane. The left wall has a wavy architecture (arrowhead). Scale bar 100  $\mu\text{m}$ . *a* anus; *ci* cilium; *g* gonad; *gc* globular cell; *i* intestine; *ls* left stomach



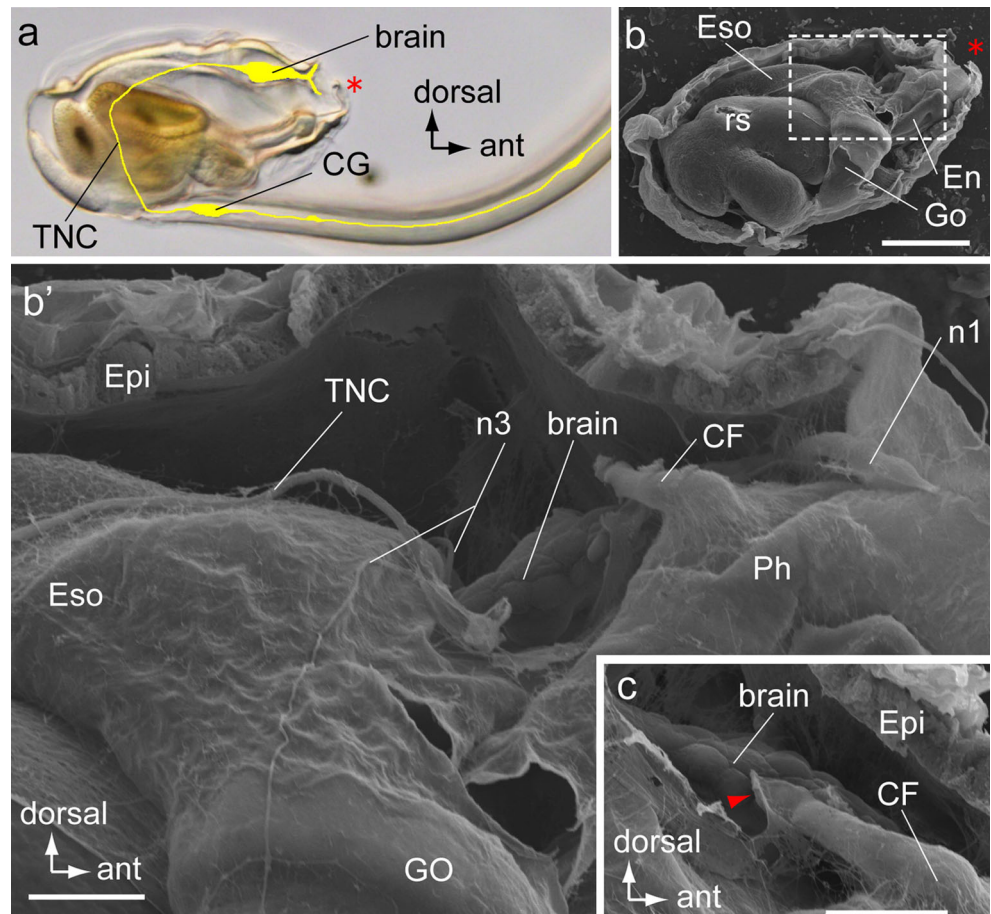
or motor functions have been described as n1–n3 (Bollner et al. 1986; Olsson et al. 1990; Cañestro et al. 2005) and these are seen in the images from this study (Fig. 6). The brain sends two thick axon fascicles anteriorly to the ventral sensory organs as the n1 nerve, bilaterally to the gill openings as the n3 nerve and posteriorly as the single TNC (Fig. 5b'). On the right side of the brain, the ciliary funnel (CF) forms a connection with the pharynx (Fig. 5c). The CF is a ciliated duct that secretes mucosa (Holmberg 1982). Accordingly, beating of the cilia in the CF is easily visible in a living animal (Supplemental Movie 3). The n1 nerves comprise a pair of thick fascicles (Fig. 6b), originating from the anterior tip of the brain (Fig. 6b). The fascicles connect with the ventral sensory organs embedded in the ventral epidermis (Fig. 6c, arrow), which were suggestive of an olfactory organ (Bollner et al. 1986; Bassham and Poslethwait 2005). The n2 nerves elongate from the middle part of the brain (Fig. 6a) and connect to the upper lip cells, lower lip cells and pharynx cells (Olsson et al. 1990). In this study, however, we could not confidently identify the n2 nerves in the SEM images. The n3 nerves are derived from the posterior portion of the brain (Fig. 6d–e). The descending axons run along the pharynx (Fig. 5b') toward the gill openings (Fig. 6e) and the axon

terminus of the n3 branch (n3br) form varicosities on the surface of the gill opening (Fig. 6e) suggesting involvement of the beating cilia (Supplemental Movie 1). Overall, these results support the plausibility of the intracerebral neural circuitry that has been established by TEM images (Bollner et al. 1986; Olsson et al. 1990).

The sensory vesicle (SV) is located on the left side of the brain (Fig. 6a). It contains a statolith (Fig. 6a) that is connected to the brain wall via a connecting shaft (Fig. 6a'), a sensory cell on the left side (Fig. 6a' arrow) and some sensory cilia (Fig. 6a', arrowheads) and thus is considered a gravity sensor, which coincides with previous studies (Holmberg 1984). In the present study, we obtained a few SEM images of the inner and outer regions of the SV that showed that the outer surface consists of a thin-membrane (Fig. 6f–g), the ventral surface adheres to the pharynx (Fig. 6h) and the inner side contains several bundles in the membrane (Fig. 6h'). These bundles are thought to be sensory cilia (Fig. 6h', arrowhead) and sensory cells (Fig. 6h', arrow).

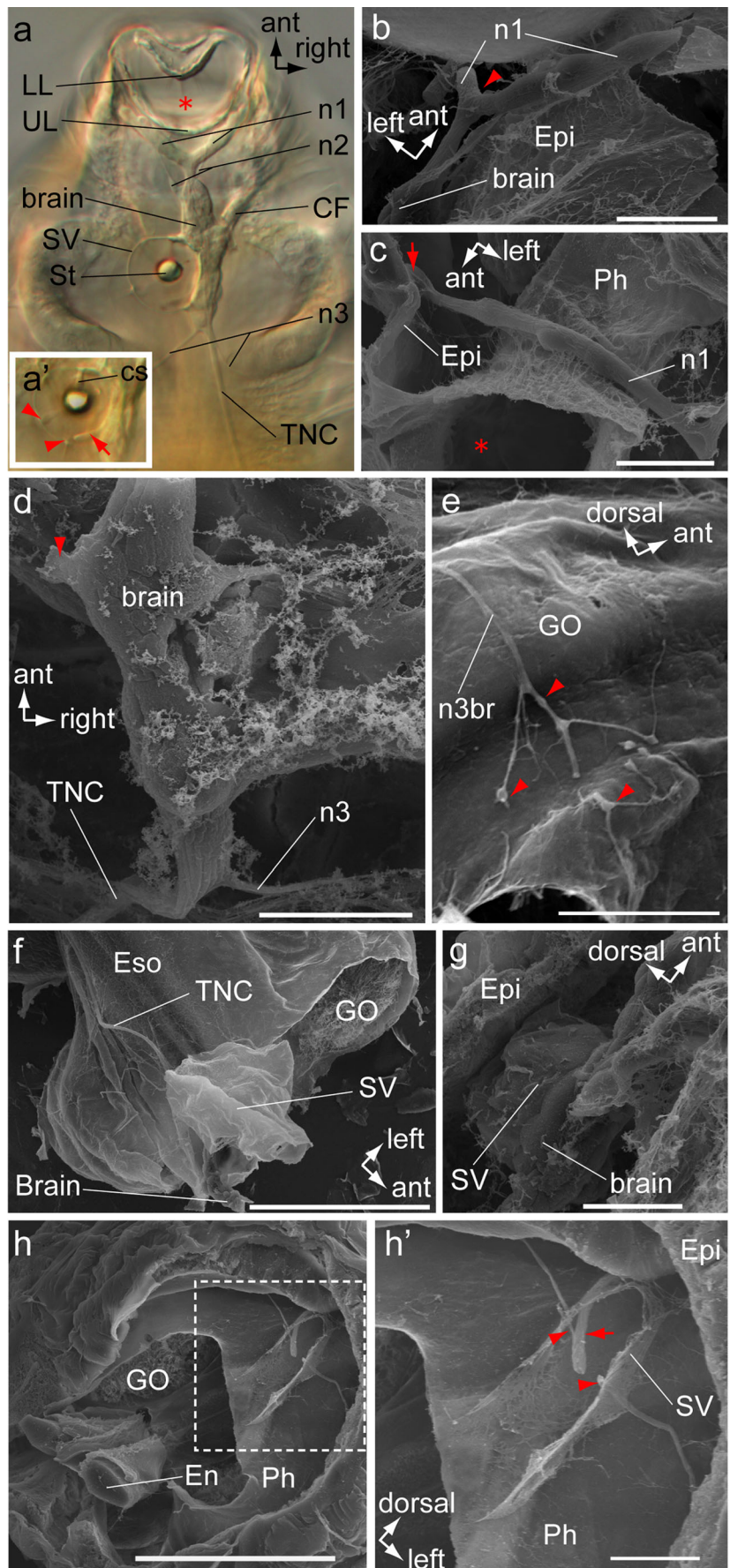
In the tail, the nerve cord from the tail ganglion (CG) runs along the left side of the notochord (Figs. 1i, 7a). The CG is located at the proximal end of the tail (Fig. 7c) and possesses a thick fascicle that elongates anteriorly (Fig. 7c'). This supports

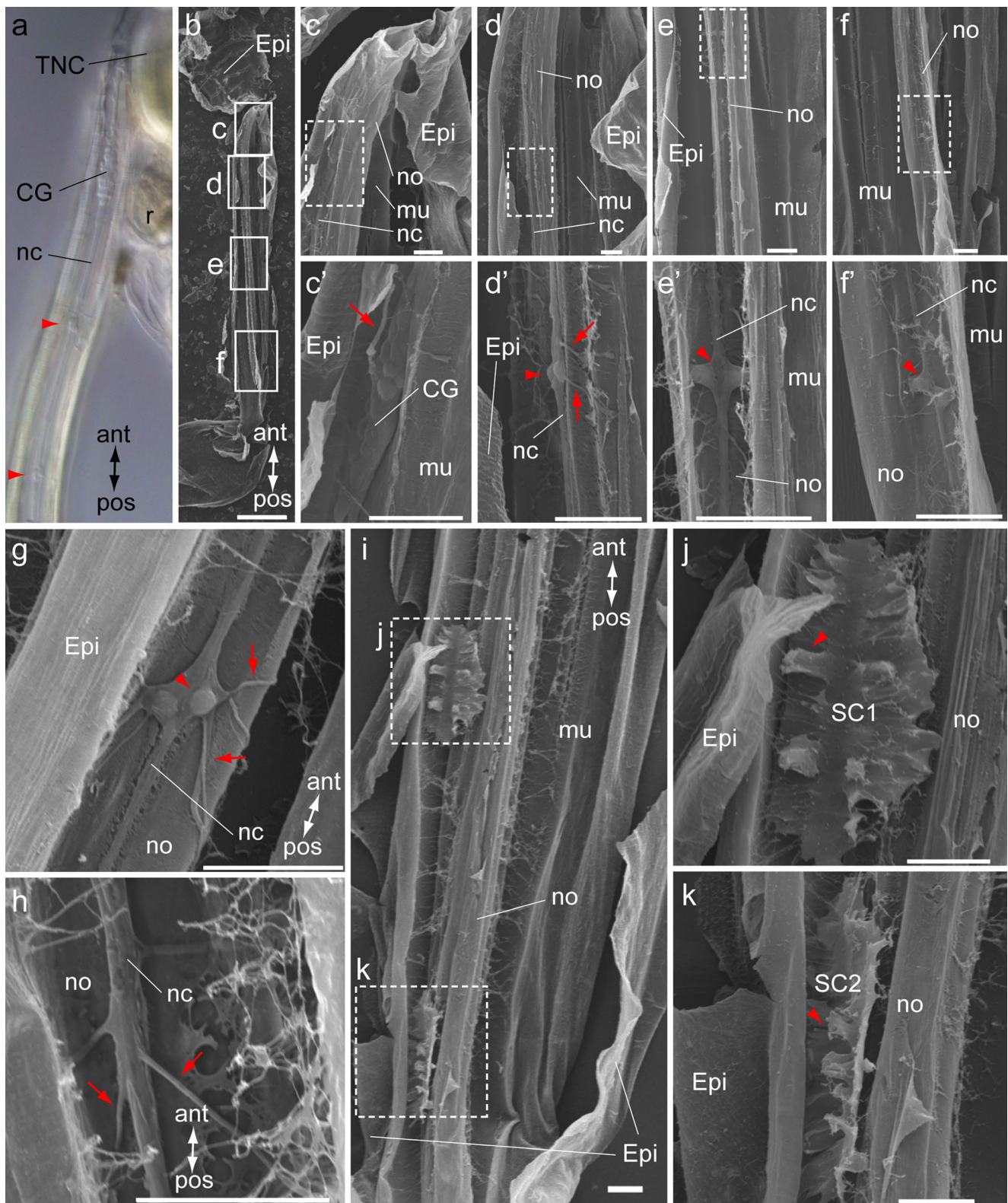
**Fig. 5** **a** Nervous system DIC image of living specimens. Right view. The brain, caudal ganglion (CG) and nerve cords are labeled with yellow. Asterisk the mouth. **b** Right view of specimens from which epidermis was removed. **b'** Close-up view of the square in (b). **c** Detailed view of the ciliary funnel (CF). Arrowhead indicates the connection between the CF and the right side of the brain. Scale bars (b) 100  $\mu$ m, (b', c) 20  $\mu$ m. CF ciliary funnel; En endostyle; Epi epidermis; Eso esophagus; GO gill opening; n1 and n3 paired nerve; Ph pharynx; rs right stomach; SV sensory vesicle; TNC trunk nerve cord





**Fig. 6** **a** Brain nerves and sensory vesicle DIC images of living specimens. Dorsal view. *Asterisk* the mouth. **a'** A merged DIC image of two different focal planes of the sensory vesicle (SV). Dorsal view. *Arrow* and *arrowheads* indicate the sensory cell and sensory cilia, respectively, which are in contact with the surface of the SV. **b, c** The pair of n1 nerves. **b** Dorsal view. *Arrowhead* represents the junction of the n1 nerve pair. **c** Anterior dorsal view. *Arrow* indicates the connection of the n1 nerve and the ventral sensory organ. **d** Dorsal view of the brain. The SV is detached at the left side (*arrowhead*). **e** A branch of the n3 nerve (*n3br*) near the gill opening (GO). *Arrowheads* indicate varicosities. **f–h** SV. **f** Dorsal view. The surface of the SV has shrunk. **g** Right view. **h** Anterior view of cutting plane in which an internal portion of the SV surface is exposed. **h'** Enlarged view of the square area in (**h**). *Arrow* represents a potential structure of the sensory cell in (**a'**). *Arrowheads* indicate cilia that have penetrated the surface of the SV. *Scale bar* (**f, h**) 100  $\mu$ m, (**b–e, g, h'**) 20  $\mu$ m. *CF* ciliary funnel; *cs* connecting shaft; *En* endostyle; *Epi* epidermis; *Eso* esophagus; *GO* gill opening; *LL* lower lip; *n1, n2* and *n3* paired brain nerves; *n3br*, a branch of the n3 nerve toward the GO; *Ph* pharynx; *St* statolith; *SV* sensory vesicle; *TNC* trunk nerve cord; *UL* upper lip





the notion that the CG makes neural connections with a pair of epidermal sensory bristles in the trunk: the Langerhans receptors (Holmberg 1986). Sporadic distributions of neuronal cell

bodies are observed at intervals (Fig. 7d–f) and are recognized as clusters of a few cells (Fig. 7a, d’–f’, g) and interpreted as ganglia. Multiple neural processes branched off the ganglia



◀ **Fig. 7** Caudal nerves and subchordal cells in the tail. **a** DIC image of living specimens. Lateral view. *Arrowheads* indicate clusters of neural somata. **b–h** Caudal nerve system. **b** An overview of specimens from which the epidermis and a part of the muscle were fractured and removed. **c–f** Close-up views of square areas in **(b)**. Images were serially collected from anterior to posterior. Portions of nerve cells (in the *dotted squares*) are enlarged and shown in **(c'–f')**. Cell bodies and nerve fibers are indicated by *arrowhead* and *arrow*, respectively. **g, h** Nerve processes from ganglion cells. These processes are derived from both somata **(g)** and nerve cord **(h)**. **i–k** Subchordal cells (SC). **i** A view of the opposite (peeled off) side of **(b)**. **j, k** Enlarged views of the square area in **(i)**. Two SCs in the anterior and posterior positions are referred to as SC1 and SC2, respectively. *Arrowheads* indicate the protrusions. Note that the notochord is somewhat caved in due to sample preparation. *Scale bars* **(b)** 200  $\mu\text{m}$ , **(c–k)** 20  $\mu\text{m}$ . *CG* caudal ganglion; *Epi* epidermis; *mu*, muscle; *nc* nerve cord; *no*, notochord; *r* rectum; *SC1* anterior subchordal cell; *SC2* posterior subchordal cell; *TNC* trunk nerve cord

(Fig. 7d', g, h) from neuronal somata (Fig. 7d', g) or from the fascicle of the nerve cord (Fig. 7h).

### Subchordal cells in the tail

Two subchordal cells (SCs) are situated on the right side of the notochord (Fig. 7i). They have a flattened shape but have a number of protrusions on the surface (Fig. 7j, k). Surface structures are variable between the first and second SCs and among observations. It is possible that the plasma membranes or intracellular compartments reshape in living animals. Indeed, live imaging of SC precursors in newly hatched larvae has shown the presence of lamellapodium-like protrusions (Kishi et al. 2014). In appendicularians, SCs exist only in the genera *Oikopleura*, *Stegosoma* and *Folia*, which also possess oral gland cells in the trunk (Fredriksson and Olsson 1991). Species lacking the oral gland do not have SCs. The subchordal cells have been proposed to have a relationship with the oral gland. Our results, however, showed that these cells are distinct in terms of morphology. The oral gland has a roundish shape and smooth surface (Fig. 3i'), whereas the SCs have a flattened shape and many protrusions on the surface. These results are in accordance with the DIC microscopic observation of larvae (Kishi et al. 2014). The relationship between ontogenetic origins and morphological aspects of SCs and the oral gland is an open question and awaits future clarification.

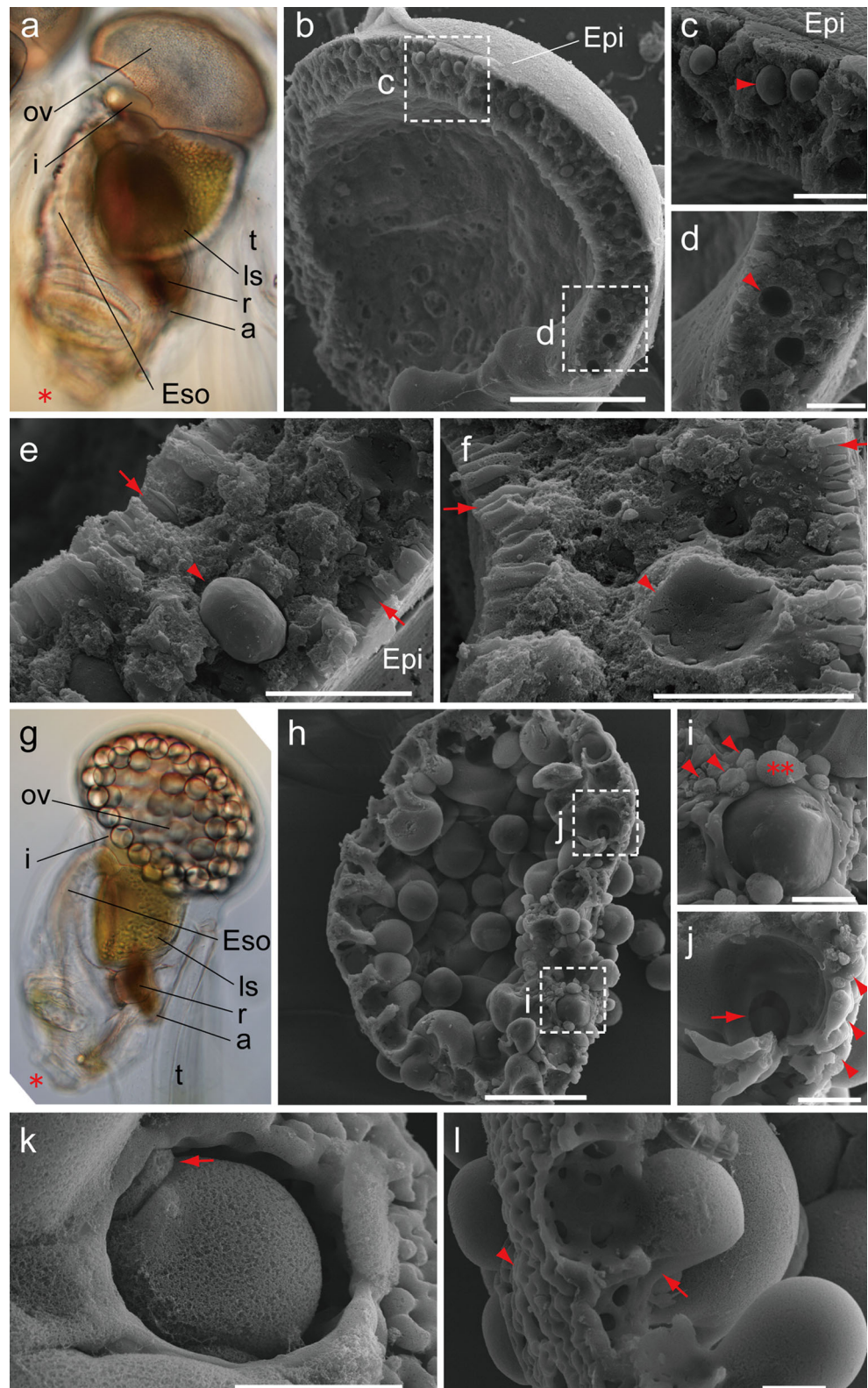
### Gametogenesis in the ovary and testis

The ovary and testis were investigated with reference to gametogenesis (Figs. 8, 9). Formation of the oocyte or sperm is rapid, taking only several hours (Nishino and Morisawa 1998). The whole ovary is a single syncytium (called a coenocyte) and contains a substantial numbers of meiotic and nurse nuclei (Fig. 8b). Oogenesis has been proposed to occur in a rather unusual manner (Ganot et al. 2006, 2007) in that

nuclei are enclosed in growing oocytes that are interconnected to the common cytoplasm via a pole, called the ring canal. Some meiotic nuclei are selected as pro-oocytes and most of the ovarian common cytoplasm is introduced into them over several hours of oogenesis. Non-selected nuclei and nurse nuclei then undergo apoptosis (Ganot et al. 2007). Based on this background, we investigated the internal structures. In the early stage of oogenesis as seen in this study, the ovary is relatively thin and thus forms a central cavity adjacent to the intestine (Fig. 8a, b). It is enclosed within a thin monolayer of follicular epithelium surrounding the central region of the germline (Fig. 8b). In the cut surfaces, many pro-oocytes (Fig. 8c, e) and spherical holes, from which the pro-oocytes are removed, are visible (Fig. 8d, f) in the central but not peripheral, regions of the cutting planes. In the late stage of oogenesis, growing oocytes are clearly visible in the ovary (Fig. 8g, h) and they are surrounded with small and unselected pro-oocytes (Fig. 8i) and aggregations of sphere materials (Fig. 8i, j). These materials are likely to contain unselected pro-oocytes and/or nurse nuclei. It is less likely that growing oocytes are surrounded by smaller pro-oocytes, because oocytes grow in a synchronous manner and females spawn all eggs only once in lifetime. This notion is also supported by confocal microscopic observation of the ovary (Ganot et al. 2006, 2007). Traces of ring canal are visible in the hollows where growing oocytes were located (Fig. 8j) and each growing oocyte has a single junction with the common cytoplasm (Fig. 8k, l). Nurse nuclei are interconnected forming a large aggregation (Fig. 8).

A novel observation was made of column-like structures that occupy a majority of the subcortical regions of the ovary in the early stage of oogenesis (Fig. 8e, f, arrows). The superficial end of the column is adjacent to either the ovarian cavity or follicular epithelium (Fig. 8e). In contrast, the deeper end of the column is unclear because it appeared to fuse with the common cytoplasm (Fig. 8f). These results not only support but also complement the abovementioned model of oogenesis (Ganot et al. 2007). In the model, the cortical membrane invaginates into the common cytoplasm to form the oocyte membrane (Ganot et al. 2007). Confocal microscopic observations have revealed that plasma membrane and F-actin form networks in the cortical areas (Ganot et al. 2006; 2007). The density and orientation of the invagination are unclear and not mentioned in these studies; however, in the present study, it was clearly demonstrated that the invagination occurs in a direction almost orthogonal to the ovarian surface. However, it is also noted that the number of invaginations is too many provided that all of them connected to oocyte membranes. *Oikopleura dioica* usually spawn less than 300 eggs; however, 10–20 invaginations occurred per 10  $\mu\text{m}$  of the cutting plane (Fig. 8e, f), implying the formation of thousands of oocytes. At present, we do not have a clear explanation for this discrepancy.

**Fig. 8** Ovary and oogenesis. **a–f** Early stage of oogenesis. **a** DIC image of living specimens. Lateral view. *Asterisk* the mouth. **b–f** Cut surfaces. **b** A low-resolution overview. **c, d** Enlarged views of the square area in **(b)**. **e, f** Detailed internal structures. *Arrowheads* indicate growing oocytes (**c, e**) or their traces (**d, f**). *Arrows* represent the column-like structures in both sides of the peripheral ovary. **g–l** Late stage of oogenesis. **g** DIC image of living specimens. Lateral view. *Asterisk* the mouth. **h–l** Cut surfaces. **h** A low-resolution overview. **i, j** Enlarged views of the *square area* in **(h)**. **k, l** Detailed views of growing oocytes. Unselected and not growing oocyte is labeled with a *double asterisk*. *Arrowheads* indicate aggregations of unselected oocytes and/or nurse nuclei. *Arrows* indicate ring canals connecting growing oocyte and ovarian common cytoplasm. *Scale bars* (**b, h**) 100  $\mu$ m, (**c–f, i–l**) 20  $\mu$ m. *a* anus; *Epi* epidermis; *Eso* esophagus; *i* intestine; *ls* left stomach; *ov* ovary; *r* rectum; *t* tail

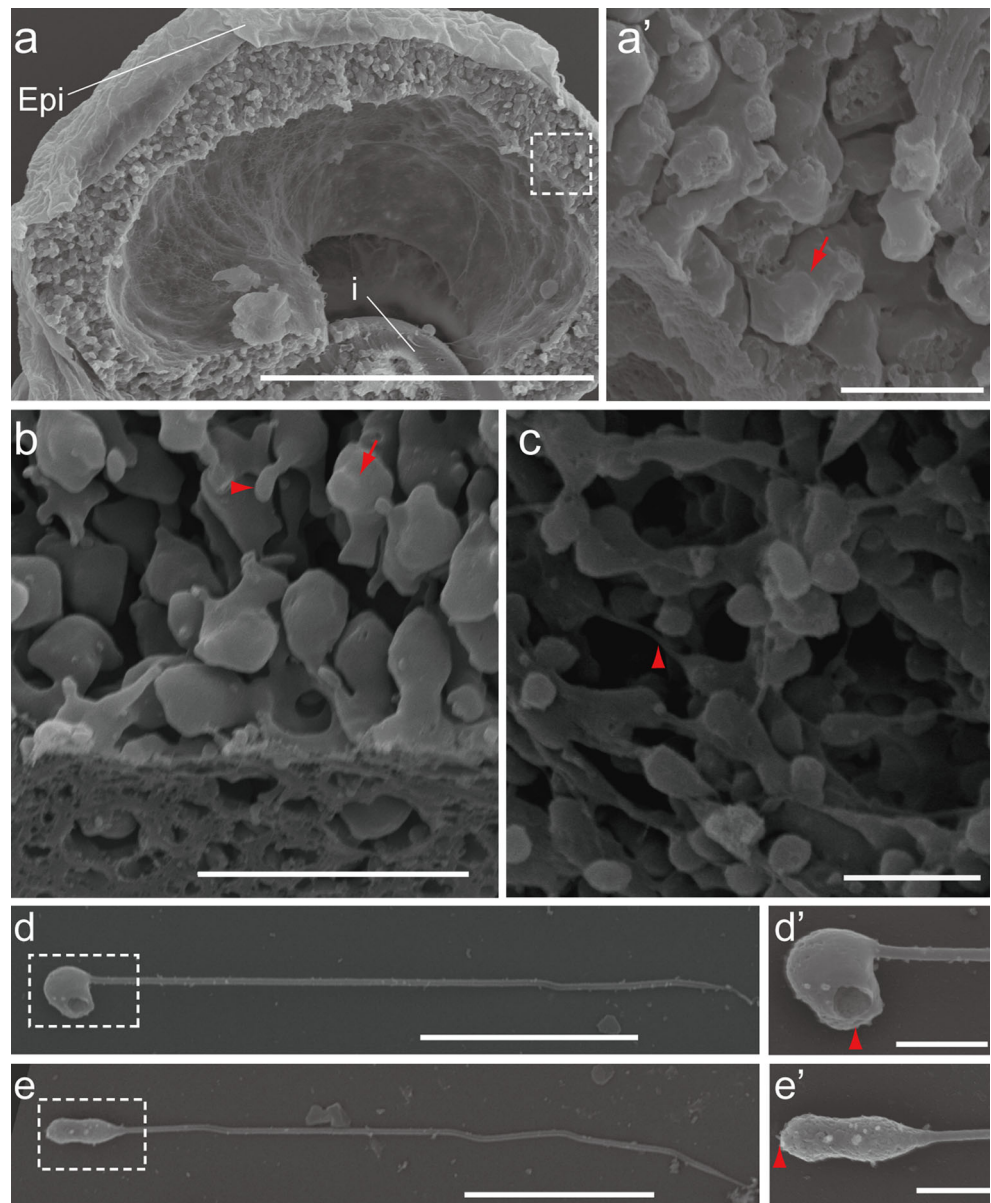


The testis is recognized as a single syncytium that interconnects a substantial number of gamete nuclei (Fig. 9a–c). Spermatogenesis occurs in a rather

synchronized way (Fig. 9). Here, it was categorized as the early, intermediate and late stage, each separated by approximately 4-hour periods (Fig. 9a–c). In the early



**Fig. 9** Testis and spermatogenesis. **a–c** Inside views of the testis at the early stage (**a**), intermediate stage (**b**) and late stage (**c**) of spermatogenesis. **a'** Detailed view of the *square area* in (**b**). *Arrowheads* indicate processes corresponding to the tail of spermatids. *Arrows* represent characteristic swellings on the surface. **d, e** Maturing (**d**) and matured spermatozoa (**e**). (**d'**, **e'**) Head regions are shown. *Arrowheads* indicate anterior tip where the acrosome exists. *Scale bars* (**a**) 50  $\mu\text{m}$ , (**a'**, **b**, **c**, **d**, **e**) 5  $\mu\text{m}$ , (**d'**, **e'**) 1  $\mu\text{m}$ . *Epi* epidermis; *i* intestine



stage, the testis is composed of sinuous and interconnected lobes (Fig. 9a') with a relatively smooth surface. A portion of the lobes is swollen on the surface (Fig. 9a', b). This result is reminiscent of TEM observations of meiotic spermatocytes, which are characteristic of nuclei and centriole protrusions (Martinucci et al. 2005). In the intermediate stage of spermatogenesis, the formation of sperm tails is observed in each lobe (Fig. 9b). The tails contain flagella on the surface and swollen areas indicate that the meiotic nuclei/centrioles are still evident on the surface (Fig. 9b). In the late stage, the whole testis comprises clusters of spermatids (Fig. 9c) and each cell body contains long flagella (Fig. 9c). These observations support the claim that all nuclei are transferred into

spermatozoa and that no nurse nuclei exist in males of the family Oikoleuridae (Martinucci et al. 2005).

Spermatozoa are approximately 20  $\mu\text{m}$  in length from head to tail (Fig. 9d, e). Two types of sperm cells are found in the nearly mature testis: spermatids (Fig. 9d) and spermatozoa (Fig. 9e). In spermatids, the tail is bent along the anterior-posterior axis of the head (Fig. 9d). In contrast, spermatozoa have a stereotypical sperm shape (Fig. 9e). In spermatids, the anterior tip of the head is depressed (Fig. 9d) and this part is considered to be the gap between the acrosome and basal body as implicated by TEM and SEM observations (Flood 1975). This study, however, could not observe acrosomes or basal bodies with SEM. This discrepancy is explained by the fact that

they used air-dried specimens for SEM observation, whereas we processed specimens via critical point drying. The depressed part of the spermatid head is no longer observed in the spermatozoa (Fig. 9e’).

## Summary

In summary, an SEM atlas of adult *Oikopleura dioica* was generated. It covers nearly all internal organs and external morphology including (1) the epidermis, (2) the pharynx and digestive tract, (3) the heart, (4) the nervous system and (5) gametogenesis in the ovary and testis. Our results not only complement previous knowledge but also reveal novel aspects of the functional anatomy of adults of this species. For instance, observation of the digestive tract unraveled a left–right asymmetry in the trigeminal passage toward the esophagus and gill openings and morphologically distinct endostyle with a ciliated band spanning the ventro-anterior to posterior region. This study provides clear SEM images showing that the brain connects to various organs and also the internal structure of the SV. Furthermore, SEM observations revealed that an excess number of membrane invaginations are formed in the cortical parts of the ovary during the early phases of oogenesis. The comprehensive 3D atlas outlined here will provide a valuable reference for studying development and physiology using this simple organism with a chordate body plan.

**Acknowledgments** We thank M. Suzuki and several students at Osaka University for their help with the culture of *O. dioica*. K. Hayashi contributed preliminary tests for SEM observation. We also appreciate the Research Management and Administration Section at Osaka University for proofreading the manuscript. This work was supported by a Grant-in-Aid for Scientific Research from the JSPS to HN (22370078, 26650079, 15H04377 and 16K14735) and TAO (24870019 and 26840079). TAO is supported by research grants from the Inamori Foundation (2015) and the Kato Memorial Research Foundation (2015–2016).

## References

- Bassham, Poslethwait JH (2005) The evolutionary history of placodes: a molecular genetic investigation of the larvacena urochordate *Oikopleura dioica*. *Development* 132:4259–4272. doi:10.1242/dev.01973
- Bollner T, Holmberg K, Olsson R (1986) A rostral sensory mechanism in *Oikopleura dioica* (Appendicularia). *Acta Zool* 67:235–241. doi:10.1111/j.1463-6395.1986.tb00868.x
- Bouquet JM, Spriet E, Troedsson C, Ottera H, Chourrout D, Thompson EM (2009) Culture optimization for the emergent zooplanktonic model organism *Oikopleura dioica*. *J Plankton Res* 31:359–370. doi:10.1093/plankt/fbn132
- Burighel P, Brena C (2001) Gut ultrastructure of the appendicularian *Oikopleura dioica* (Tunicata). *Invertebr Biol* 120:278–293. doi:10.1111/j.1744-7410.2001.tb00038.x
- Burighel P, Lane NJ, Martinucci GB, Fenaux R, Dallai R (1989) Junctional diversity in two regions of the epidermis of *Oikopleura dioica* (Tunicata, Larvacea). *Cell Tissue Res* 257:529–535. doi:10.1007/bf00221462
- Cañestro C, Bassham S, Postlethwait J (2005) Development of the central nervous system in the larvacena *Oikopleura dioica* and the evolution of the chordate brain. *Dev Biol* 285:298–315. doi:10.1016/j.ydbio.2005.06.039
- Cañestro C, Bassham S, Postlethwait JH (2008) Evolution of the thyroid: anterior-posterior regionalization of the *Oikopleura* endostyle revealed by Otx, Pax2/5/8, and Hox1 expression. *Dev Dyn* 237:1490–1499. doi:10.1002/dvdy.21525
- Clarke T, Bouquet JM, Fu X, Kallese T, Schmid M, Thompson EM (2007) Rapidly evolving lamins in a chordate, *Oikopleura dioica*, with unusual nuclear architecture. *Gene* 396:159–169. doi:10.1016/j.ajhg.2013.10.020
- Danks G, Campsteijn C, Parida M, Butcher S, Doddapaneni H, Fu B, Petrin R, Metpally R, Lenhard B, Wincker P, Chourrout D, Thompson EM, Manak JR (2013) OikoBase: a genomics and developmental transcriptomics resource for the urochordate *Oikopleura dioica*. *Nucleic Acids Res* 41:1–9. doi:10.1093/nar/gks1159
- De Souza W, Campanati L, Attias M (2008) Strategies and results of field emission scanning electron microscopy (FE-SEM) in the study of parasitic protozoa. *Micron* 39:77–87. doi:10.1016/j.micron.2006.11.003
- Delsuc F, Brinkmann H, Chourrout D, Philippe H (2006) Tunicates and not cephalochordates are the closest living relatives of vertebrates. *Nature* 439:965–968. doi:10.1038/nature04336
- Denoeud F, Henriot S, Mungpakdee S, Aury JM, Da Silva C, Brinkmann H, Mikhaleva J, Olsen LC, Jubin C, Canestro C, Bouquet JM, Danks G, Poulain J, Campsteijn C, Adamski M, Cross I, Yadete F, Muffato M, Louis A, Butcher S, Tsagkogeorga G, Konrad A, Singh S, Jensen MF, Cong EH, Eikeseth-Otterra H, Noel B, Anthouard V, Porcel BM, Kachouri-Lafond R, Nishino A, Ugolini M, Chourrout P, Nishida H, Aasland R, Huzurbazar S, Westhof E, Delsuc F, Lehrach H, Reinhardt R, Weissenbach J, Roy SW, Artiguenave F, Postlethwait JH, Manak JR, Thompson EM, Jaillon O, Du Pasquier L, Boudinot P, Liberles DA, Volff JN, Philippe H, Lenhard B, Crollius HR, Wincker P, Chourrout D (2010) Plasticity of animal genome architecture unmasked by rapid evolution of a pelagic tunicate. *Science* 330:1381–1385. doi:10.1126/science.1194167
- Fenaux R (1998) Anatomy and functional morphology of the Appendicularia. In: Bone Q (ed) *The biology of pelagic tunicates*. Oxford University Press, New York, pp 25–34
- Flood PR (1975) Scanning electron microscope observations on the muscle innervation of *Oikopleura dioica* Fol (appendicularia, tunicata) with notes on the arrangement of connective tissue fibres. *Cell Tissue Res* 164:357–369. doi:10.1007/bf00223014
- Flood PR (1978) The spermatozoon of *Oikopleura dioica* Fol (Larvacea, Tunicata). *Cell Tissue Res* 191:27–37. doi:10.1007/bf00223213
- Fredriksson G, Olsson R (1991) The subchordal cells of *Oikopleura dioica* and *O. albicans* (Appendicularia, Chordata). *Acta Zool* 72:251–256. doi:10.1111/j.1463-6395.1991.tb01203.x
- Fredriksson G, Ofverholm T, Ericson LE (1985) Ultrastructural demonstration of iodine binding and peroxidase activity in the endostyle of *Oikopleura dioica* (Appendicularia). *Gen Comp Endocrinol* 58:319–327. doi:10.1016/0016-6480(85)90348-x
- Fujii S, Nishio T, Nishida H (2008) Cleavage pattern, gastrulation, and neurulation in the appendicularian, *Oikopleura dioica*. *Dev Genes Evol* 218:69–79. doi:10.1007/s00427-008-0205-4
- Ganot P, Thompson EM (2002) Patterning through differential endoreduplication in epithelial organogenesis of the chordate, *Oikopleura dioica*. *Dev Biol* 252:59–71. doi:10.1006/dbio.2002.0834
- Ganot P, Bouquet JM, Thompson EM (2006) Comparative organization of follicle, accessory cells and spawning Anlagen in dynamic semelparous clutch manipulators, the urochordate Oikopleuridae. *Biol Cell* 98:389–401. doi:10.1042/bc20060005



- Ganot P, Bouquet JM, Kallesøe T, Thompson EM (2007) The *Oikopleura* coenocyst, a unique chordate germ cell permitting rapid, extensive modulation of oocyte production. *Dev Biol* 302:591–600. doi:10.1016/j.ydbio.2006.10.021
- Holmberg K (1982) The ciliated brain duct of *Oikopleura dioica* (Tunicata, Appendicularia). *Acta Zool* 63:101–109. doi:10.1111/j.1463-6395.1982.tb00765.x
- Holmberg K (1984) A transmission electron microscopic investigation of the sensory vesicle in the brain of *Oikopleura dioica* (Appendicularia). *Zoomorphology* 104:298–303. doi:10.1007/bf00312011
- Holmberg K (1986) The neural connection between the Langerhans receptor cells and the central nervous system in *Oikopleura dioica* (Appendicularia). *Zoomorphology* 106:31–34. doi:10.1007/bf00311944
- Hosp J, Sagane Y, Danks G, Thompson EM (2012) The evolving proteome of a complex extracellular matrix, the *Oikopleura* house. *PLoS ONE* 7, e40172. doi:10.1371/journal.pone.0040172
- Kishi K, Onuma TA, Nishida H (2014) Long-distance cell migration during larval development in the appendicularian, *Oikopleura dioica*. *Dev Biol* 395:299–306. doi:10.1016/j.ydbio.2014.09.006
- Martinucci G, Brena C, Cima F, Burighel P (2005) Synchronous spermatogenesis in appendicularians. In: Gorsky G, Youngbluth MJ, Deibel D (eds) Response of marine ecosystems to global changes: ecological impact of appendicularians. Contemporary, Paris, pp 113–123
- Nakashima K, Nishino A, Hirose E (2011) Forming a tough shell via an intracellular matrix and cellular junctions in the tail epidermis of *Oikopleura dioica* (Chordata: Tunicata: Appendicularia). *Naturwissenschaften* 98:661–669. doi:10.1007/s00114-011-0815-y
- Nishida H (2008) Development of the appendicularian *Oikopleura dioica*: Culture, genome, and cell lineages. *Develop Growth Differ* 50:S239–S256
- Nishida H, Stach T (2014) Cell lineages and fate maps in tunicates: conservation and modification. *Zool Sci* 31:645–652. doi:10.1111/j.1440-169x.2008.01035.x
- Nishino A, Morisawa M (1998) Rapid oocyte growth and artificial fertilization of the Larvaceans *Oikopleura dioica* and *Oikopleura longicauda*. *Zool Sci* 15:723–727. doi:10.2108/zsj.15.723
- Olsson R (1965) The cytology of the endostyle of *Oikopleura dioica*. *Ann N Y Acad Sci* 118:1038. doi:10.1111/j.1749-6632.1965.tb40170.x
- Olsson R, Holmberg K, Lilliemarck Y (1990) Fine structure of the brain and brain nerves of *Oikopleura dioica* (Urochordata, Appendicularia). *Zoomorphology* 110:1–7. doi:10.1007/bf01632806
- Omotezako T, Nishino A, Onuma TA, Nishida H (2013) RNA interference in the appendicularian *Oikopleura dioica* reveals the function of the Brachyury gene. *Dev Genes Evol* 223:261–267. doi:10.1007/s00427-013-0438-8
- Omotezako T, Onuma TA, Nishida H (2015) DNA interference: DNA-induced gene silencing in the appendicularian *Oikopleura dioica*. *Proc R Soc Lond B* 282:20150435. doi:10.1098/rspb.2015.0435
- Sagane Y, Zech K, Bouquet JM, Schmid M, Bal U, Thompson EM (2010) Functional specialization of cellulose synthase genes of prokaryotic origin in chordate larvaceans. *Development* 137:1483–1492. doi:10.1242/dev.044503
- Seo HC, Kube M, Edvardsen RB, Jensen MF, Beck A, Spriet E, Gorsky G, Thompson EM, Lehrach H, Rienhardt R, Chourrout D (2001) Miniature Genome in the Marine Chordate *Oikopleura dioica*. *Science* 294:2506. doi:10.1126/science.294.5551.2506
- Søviknes AM, Chourrout D, Glover JC (2005) Development of putative GABAergic neurons in the appendicularian urochordate *Oikopleura dioica*. *J Comp Neurol* 490:12–28. doi:10.1002/cne.20629
- Søviknes AM, Chourrout D, Glover JC (2007) Development of the caudal nerve cord, motoneurons, and muscle innervation in the appendicularian urochordate *Oikopleura dioica*. *J Comp Neurol* 503:224–243. doi:10.1002/cne.21376
- Stach T, Anselmi C (2015) High-precision morphology: bifocal 4D-microscopy enables the comparison of detailed cell lineages of two chordate species separated for more than 525 million years. *BMC Biol* 13:113. doi:10.1186/s12915-015-0218-1
- Stach T, Winter J, Bouquet JM, Chourrout D, Schnabel R (2008) Embryology of a planktonic tunicate reveals traces of sessility. *Proc Natl Acad Sci U S A* 105:7229–7234. doi:10.1073/pnas.0710196105
- Troedsson C, Ganot P, Bouquet JM, Aksnes DL, Thompson EM (2007) Endostyle cell recruitment as a frame of reference for development and growth in the urochordate *Oikopleura dioica*. *Biol Bull* 213:325–334. doi:10.2307/25066650
- Wang K, Omotezako T, Kishi K, Nishida H, Onuma TA (2015) Maternal and zygotic transcriptomes in the appendicularian, *Oikopleura dioica*: novel protein-encoding genes, intra-species sequence variations, and trans-spliced RNA leader. *Dev Genes Evol* 225:149–159. doi:10.1007/s00427-015-0502-7